

# Chaotic mixing of complex fluids: on the effects of viscosity ratio

Mohammad Reza Daneshvar Garmroodi

Dept. of Mechanical, Industrial & Aerospace Engineering  
 Concordia University  
 Montreal, Quebec  
 mohammadreza.daneshvargarmroodi@concordia.ca

Ida Karimfazli

Dept. of Mechanical, Industrial & Aerospace Engineering  
 Concordia University  
 Montreal, Quebec  
 ida.karimfazli@concordia.ca

**Abstract**—We study the evolution of chaotic mixing in an initially stratified circular vessel. The bottom and top halves of the vessel are filled with viscoplastic and Newtonian fluids. A circular stirrer in the vessel promotes the mixing. We considered three different viscosity ratios to understand the effect of viscosity on the mixing evolution. The results reveal that as the viscosity ratio increases, the mixed region shrinks, and more time is required for mixing.

**Index Terms**—Chaotic mixing, Laminar flow, Multiphase, Viscoplastic fluids, Yield stress.

## I. INTRODUCTION

Mixing is a common process in various industries. Food, pharmaceutical, wastewater treatment, and oil industry are some examples where different fluids need to be mixed together. Turbulent flow has been the favorite choice for mixing processes. However, in many applications, where working fluids are highly viscous, reaching turbulent mixing is impossible or requires a lot of energy which is not economical. In such situations, chaotic mixing is an alternative to turbulent mixing. Chaotic advection (or mixing) is defined as repeated stretching and folding of fluid filaments. Compared to turbulent mixing with considerable velocity fluctuations, chaotic mixing has a spatially smooth velocity field [1].

In most previous studies on chaotic mixing, working fluid is assumed to be homogeneous [2], [3]. In these studies, the mixing is evaluated using a passive concentration field. Gouillart et al. [4] studied the chaotic mixing of a dye blob in a Newtonian fluid numerically and experimentally. The flow regime was Stokes, and the mixing vessel was circular. They observed that the chaotic region gradually expands to the entire domain. Furthermore, it was found that the vessel wall strongly influences the dye's concentration field. They proposed a reduced model for the evaluation of concentration. In another study, Boujlel et al. [5] experimentally and numerically studied the rate of chaotic mixing in a homogeneous viscoplastic fluid. They studied the dispersion of a blob of dye in a cylindrical vessel for different values of the yield stress. They found that the mixing rate is proportional to the volume of highly sheared regions. Moreover, they proposed a quantitative two zones model to predict mixing.

There are limited studies on the mixing of inhomogeneous fluids. Derksen [6] numerically investigated the turbulent

mixing of two miscible liquids, initially stratified in a container. The fluids were Newtonian with different viscosity and densities. He used Richardson number to characterize density difference. He found that in his range of study, the viscosity ratio has a small impact on the mixing time.

In the present study, we consider mixing an inhomogeneous non-Newtonian fluid. The top and bottom halves of the domains are filled with light Newtonian and heavy viscoplastic fluids, respectively. We conduct numerical simulations to investigate the effect of the viscosity ratio on flow development and mixing evolution.

## II. PROBLEM SETUP

### A. Model problem

To study chaotic mixing, we consider a circular vessel with a stirrer that moves in a circular path with a constant angular velocity,  $\hat{\Omega}$  (see Fig. 1). The radii of vessel, circular path, and rotating stirrer are  $\hat{R}$ ,  $\hat{r}_o$ , and  $\hat{r}_s$ , respectively. The direction of the acceleration of gravity is also shown as  $\hat{g}$ . Initially, the bottom and top halves of the vessel are filled with the miscible viscoplastic and Newtonian fluids, respectively. At the vessel's wall, the no-slip boundary condition is applied.

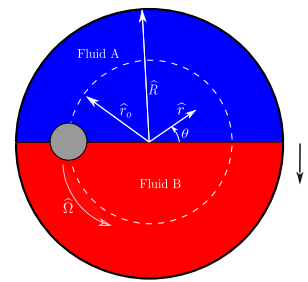


Fig. 1: Geometry in the present study

Navier-Stokes and advection-diffusion equations are coupled to model mixing of the fluid. The following non-dimensional parameters are defined:

$$\begin{aligned}
 r &= \frac{\hat{r}}{\hat{r}_o} & \mathbf{U} &= \frac{\hat{\mathbf{U}}}{\hat{r}_o \hat{\Omega}} & t &= \hat{\Omega} \hat{t} \\
 P &= \frac{\hat{P}}{\hat{\rho}_A \hat{r}_o^2 \hat{\Omega}^2} & \eta &= \frac{\hat{\eta}}{\hat{\mu}_A} & \dot{\gamma} &= \frac{\hat{\dot{\gamma}}}{\hat{\Omega}}
 \end{aligned} \tag{1}$$

The parameters with hat symbol ( $\hat{\phantom{x}}$ ) represent dimensional, and the parameters without hat symbol are non-dimensional parameters. Using the parameters in Eq. 1, the non-dimensional momentum and phase fraction equations can be written as follows:

$$[At\alpha + 1] \left( \frac{\partial \mathbf{U}}{\partial t} + \mathbf{U} \cdot \nabla \mathbf{U} \right) + \nabla P = \frac{1}{Re} \nabla \cdot \boldsymbol{\tau} - Ri \alpha \mathbf{e}_g \quad (2)$$

$$\frac{\partial \alpha}{\partial t} + \nabla \cdot (\mathbf{U}\alpha) + \frac{1}{At} \nabla \cdot \mathbf{U} - \frac{1}{Pe} \nabla \cdot (\nabla \alpha) = 0 \quad (3)$$

where  $\alpha$  is the phase fraction, which can be written as a function of densities,  $\alpha = \frac{\hat{\rho} - \hat{\rho}_A}{\hat{\rho}_B - \hat{\rho}_A}$ . Using this definition,  $\alpha = 0$  corresponds to pure fluid A and  $\alpha = 1$  represents pure fluid B.

$At$  is the Atwood number, which shows the dimensionless density difference between two fluids:

$$At = \frac{\hat{\rho}_B - \hat{\rho}_A}{\hat{\rho}_A} \quad (4)$$

The dimensionless shear stress and viscosity are defined as follows:

$$\tau_{ij} = \eta \dot{\gamma}_{ij} \quad (5)$$

$$\eta = \frac{(1 - \alpha)\hat{\mu}_A + \alpha\hat{\eta}_B}{\hat{\mu}_A} \quad (6)$$

Since fluid B is a viscoplastic fluid, its dimensionless viscosity is:

$$\eta_B = \frac{\hat{\eta}_B}{\hat{\mu}_A} = n + \frac{Bn}{\dot{\gamma}} \quad (7)$$

where  $\dot{\gamma}$ ,  $Bn = \frac{\hat{\tau}_y}{\hat{\mu}_A \hat{\Omega}}$ , and  $n = \frac{\hat{\mu}_B}{\hat{\mu}_A}$  represent the strain rate magnitude, Bingham number, and viscosity ration, respectively. Also,  $\hat{\tau}_y$  is the yield stress of fluid B. Using Eq. 7, we can rewrite Eq. 6 as follow,

$$\eta = (1 - \alpha) + \alpha \left( n + \frac{Bn}{\dot{\gamma}} \right) \quad (8)$$

$Re$ ,  $Pe$ , and  $Ri$  represent Reynolds, Peclet, and Richardson numbers, respectively,

$$Re = \frac{\hat{\rho}_A \hat{\Omega} \hat{r}_o^2}{\hat{\mu}_A} \quad Pe = \frac{\hat{\Omega} \hat{r}_o^2}{\hat{D}_m} \quad Ri = \frac{At \hat{g}}{\hat{r}_o \hat{\Omega}^2} \quad (9)$$

Reynolds number represents the ratio of inertial forces to Newtonian viscous forces, Peclet number represents the advective over diffusive phase transport, and Richardson number indicates the ratio of buoyancy to inertial forces.

We quantify mixing by defining the overall mixing index (MI) using the standard deviation of phase fraction,

$$MI(t) = 1 - \frac{\sqrt{\frac{1}{\pi(R^2 - r_s^2)} \int_0^R \int_0^{2\pi} (\alpha - \bar{\alpha})^2 r \, dr \, d\theta}}{\bar{\alpha}} \quad (10)$$

Here  $\alpha$  is the phase fraction field and  $\bar{\alpha}$  is the averaged phase fraction in the domain, which is 0.5. In order to study mixing in radial direction, we also define  $\theta$ -averaged mixing index as follow,

$$MI_\theta(t, r) = 1 - \frac{\sqrt{\frac{1}{2\pi} \int_0^{2\pi} (\alpha - \bar{\alpha})^2 d\theta}}{\bar{\alpha}} \quad (11)$$

Using this definition  $MI_\theta$  will be limited between 0 and 1.  $MI_\theta(r_o, t_o) = 0$  represents no mixing at  $(r_o, t_o)$  (i.e.,  $\alpha = 0$  or 1 for  $r = r_o$  and  $0 \leq \theta < 2\pi$ ), and  $MI_\theta = 1$  indicated that the fluid is fully mixed at  $r = r_o$  (i.e.,  $\alpha = \bar{\alpha}$  for  $r = r_o$  and  $0 \leq \theta < 2\pi$ ).

The dimensionless groups that govern the problem, along with the values considered here, are presented in Table. I.

TABLE I: Range of non-dimensional parameters

Non-dimensional numbers	Definition	Range
Reynolds ( $Re$ )	$\frac{\hat{\rho}_A \hat{\Omega} \hat{r}_o^2}{\hat{\mu}_A}$	$2.7 \times 10^2$
Peclet ( $Pe$ )	$\frac{\hat{\Omega} \hat{r}_o^2}{\hat{D}_m}$	$10^{10}$
Richardson ( $Ri$ )	$\frac{\hat{D}_m}{At \hat{g}}$	$10^{-2}$
Bingham ( $Bn$ )	$\frac{\hat{\tau}_y}{\hat{\mu}_A \hat{\Omega}}$	$5 \times 10^{-1}$
Atwood ( $At$ )	$\frac{\hat{\rho}_B - \hat{\rho}_A}{\hat{\rho}_A}$	$10^{-2}$
Viscosity ratio ( $n$ )	$\frac{\hat{\mu}_B}{\hat{\mu}_A}$	$1 - 10$
Vessel radius ( $R$ )	$\frac{\hat{\mu}_A}{\hat{R}}$	3.07
Stirrer radius ( $r_s$ )	$\frac{\hat{r}_o}{\hat{r}_s}$	$3.07 \times 10^{-1}$

## B. Numerical method

The simulations are carried out using the OpenFOAM toolbox, an open-source C++ library. OpenFOAM uses the finite volume method to discretize the governing equations. We use the modified twoLiquidMixingFoam solver, which we add the dynamic mesh utility to it. The pressure and velocity are coupled by the PIMPLE algorithm, a combination of PISO and SIMPLE methods. In all simulations, Courant-Friedrichs-Lewy number is equal to 0.025 (CFL = 0.025). We use the Crank-Nicolson time scheme, and space schemes are discretized using the second-order linear.

## C. Validation

To verify the numerical solver in the present study, we compared our results with Zare et al. [7]. They studied the injection of a heavy Newtonian fluid in a channel filled with a light viscoplastic fluid. We compared the evolution of displacing fluid and the thickness of the residual layer on the channel's wall. As can be seen in Fig. 2, the results agree well.

Furthermore, for the setup in this study, four different meshes are used to check the mesh independence of results.

The simulation The finest mesh (67000 cells) is used to calculate relative error in other meshes. Fig. 3 illustrates the evolution of mixing index and the relative error for different cell sizes. As can be seen in Fig. 3b, the relative error reduces by using the finer meshes. We used the finest mesh (67000 cells) for the simulations in the present study.

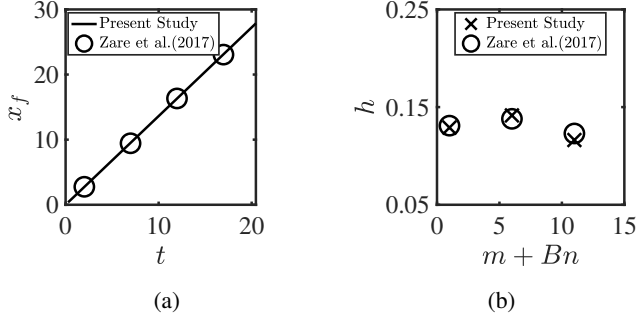


Fig. 2: (a) Evolution of displacing fluid's front position ( $x_f$ ) along the channel.  $Re = 100, \chi^* = 200, Bn = 50, m = 10$ . (b) Thickness of the residual layer on casing walls for different Bingham numbers.  $Re = 20, \chi^* = 20, m = 1$ .

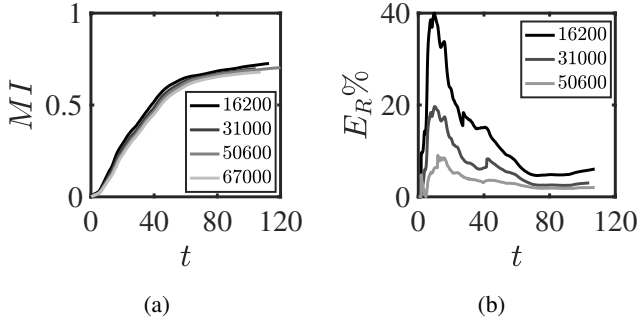


Fig. 3: (a) Evolution of mixing index for different meshes. (b) Relative error  $E_R\%$  of mixing index for different meshes based on the finest mesh.

$$(Re = 2.7 \times 10^2, Bn = 5 \times 10^{-1}, Pe = 10^{10}, Ri = 10^{-2}, At = 10^{-2}, n = 1)$$

### III. RESULTS

As an illustrative case of mixing, we present the evolution of mixing for  $n = 1$ . Fig. 4 and 5 represent the snapshots of phase fraction and vleocity magnitude, respectively. As the stirrer starts rotating in its circular path, it drags some amount of fluid A into fluid B. Due to the formation of a wake region behind the stirrer, two fluids start mixing together (see Fig. 4a). As the stirrer continues rotating, this time, the vortical region behind the stirrer drags fluid B into fluid A (see Fig. 4b). The formation of vortices can be observed in Fig. 5b. This repeating folding and stretching of fluid filaments lead to the formation of a region with chaotic mixing (see Fig. 4c). The mixing process continues until the phase fraction becomes almost uniform in the chaotic region (see Fig. 4f). After this

stage, the mixing continues mainly by diffusion between the mixed and unmixed region (a thin region near the vessel's wall).

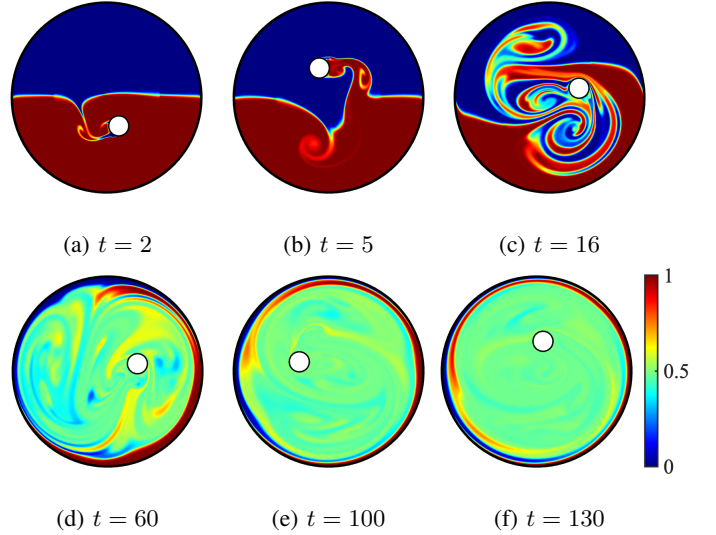


Fig. 4: Snapshots of the phase fraction at different times. ( $Re = 2.7 \times 10^2, Bn = 5 \times 10^{-1}, Pe = 10^{10}, Ri = 10^{-2}, At = 10^{-2}, n = 1$ )

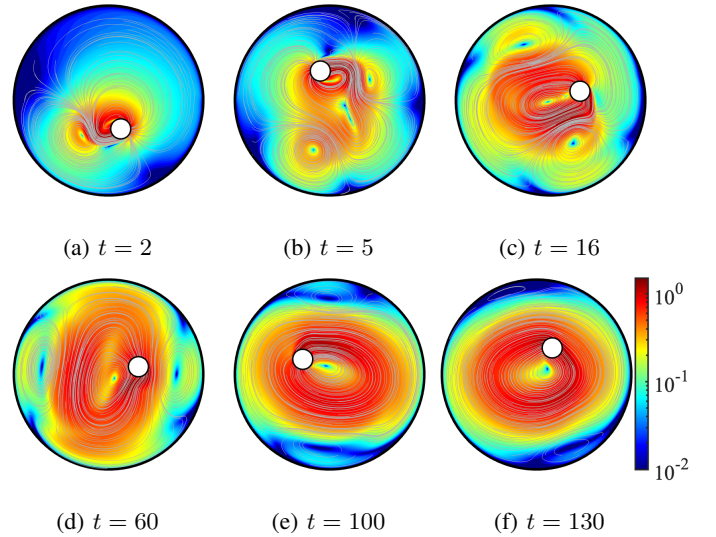


Fig. 5: Snapshots of the velocity magnitude at different times. The gray lines represent the streamlines.

$$(Re = 2.7 \times 10^2, Bn = 5 \times 10^{-1}, Pe = 10^{10}, Ri = 10^{-2}, At = 10^{-2}, n = 1)$$

Fig. 6a illustrates the evolution of mixing index. As can be seen, there is a rapid growth in  $MI$  due to chaotic mixing (until  $t \approx 70$ ). Afterward, the rate of  $MI$  decreases and mixing continues mainly by diffusion. The evolution of radial mixing is illustrated in Fig. 6b. The figure shows the spatio-temporal diagram of  $\theta$ -averaged mixing index.

For a quantitative measurement of the size of the mixed region, we have defined  $r_m$ , the averaged radius of the boundary between mixed and un-mixed regions in a quasi-steady state. Since  $MI_\theta$  changes between 0 (no mixing) to 1 (fully mixed),  $MI_\theta = 0.6$  is chosen as the boundary between these two regions, which is shown by the black dashed line (see Fig. 6b). We can see that at  $r_m \approx 2.8$ , the boundary remains almost constant, which indicates that the radial mixing reaches a quasi-steady state. Furthermore, Fig. 6c illustrates the distribution of  $MI_\theta$  along the  $r$ -direction in different time instances and the dashed line shows  $r_m$ . We can see that below the  $r_m$ , the mixing index gradually increases and becomes uniform (mixing region), while beyond the boundary, the mixing index remains almost unchanged (un-mixed region).

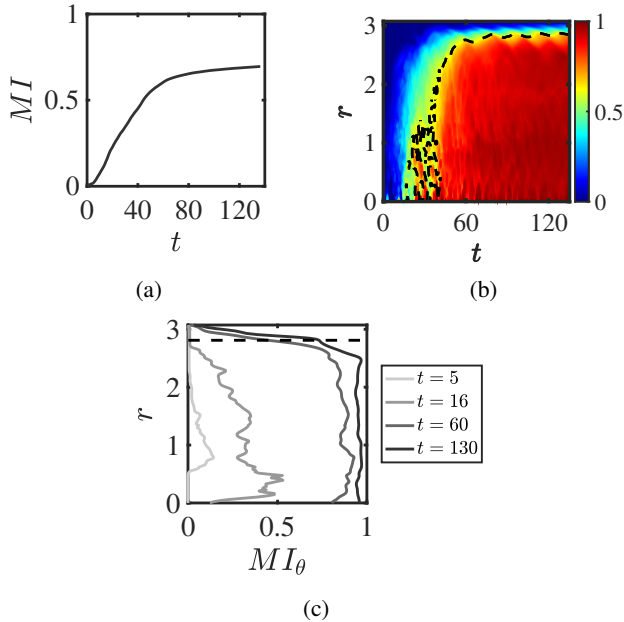


Fig. 6: (a) Evolution of overall mixing index. (b) Spatio-temporal diagram of  $\theta$ -averaged mixing index. The dash line represents  $MI_\theta = 0.6$ , which distincts the mixed and un-mixed regions. (c) Distribution of  $MI_\theta$  along the  $r$ -direction in different time instances.

$$(Re = 2.7 \times 10^2, Bn = 5 \times 10^{-1}, Pe = 10^{10}, Ri = 10^{-2}, At = 10^{-2}, n = 1)$$

#### A. Effect of viscosity ratio

To explore the effect of viscosity ratio ( $n$ ), we consider three different values including  $n = 1, 5$ , and  $10$ . Fig. 7 and 8 illustrate the evolution of phase fraction and velocity magnitude in different viscosity ratios. At the viscosity ratio  $n = 1$ , a series of vortices are formed by the stirrer's movement. The vortices stretch and fold the fluid's filaments as they advect in the domain, enhancing chaotic mixing (Fig. 7a and 8a). As the viscosity ratio increases, highly sheared zones shrink, starting from the vessel's wall (see Fig. 8b, 8e, and 8h). Therefore, the vortices near the vessel's wall become weaker, and the chaotic zone gradually becomes limited to the regions

closer to the circular path of the stirrer (see Fig. 7b, 7e, and 7h). As mixing continues, the mixed and unmixed regions in the quasi-steady state can be observed. Increasing viscosity ratio results in the shrinkage of the mixed region and growing the unmixed region around the vessel's wall (see Fig. 7c, 7f, and 7i).

Fig. 9 illustrates the evolution of the overall mixing index for different viscosity ratios. As viscosity ratios increase, the overall mixing index drops, which means more time is required to reach the desired amount of mixing.

The spatio-temporal diagrams of  $\theta$ -averaged mixing index are represented by Fig. 10. Fig. 10d shows  $r_m$  in different viscosity ratios. As  $n$  increases, radius of the mixed region reduces.

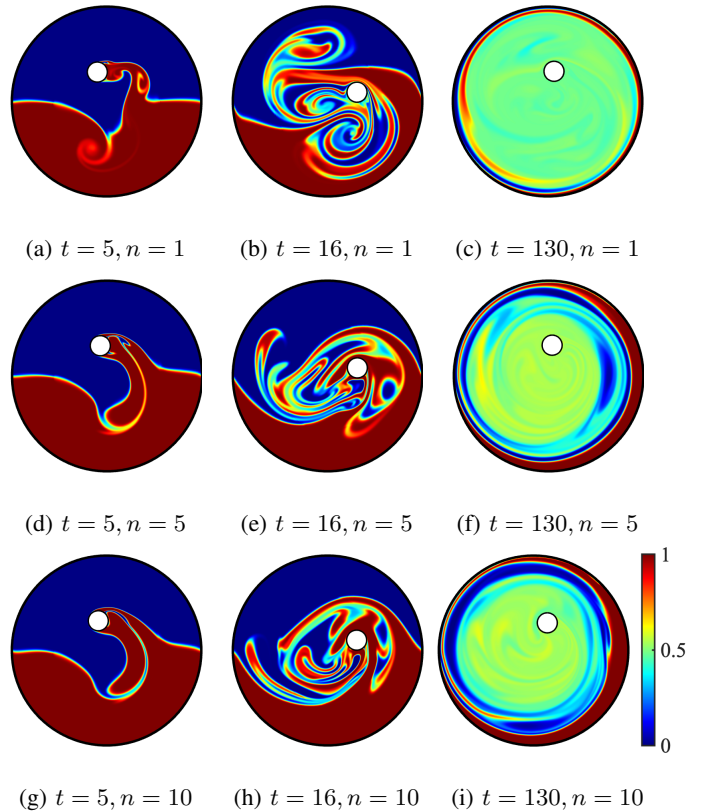


Fig. 7: Snapshots of the phase fraction for different viscosity ratios.

$$(Re = 2.7 \times 10^2, Bn = 5 \times 10^{-1}, Pe = 10^{10}, Ri = 10^{-2}, At = 10^{-2})$$

## IV. CONCLUSION

This study has explored an illustrative case of chaotic mixing of an inhomogeneous fluid in a circular vessel. We consider mixing in a 2D circular domain using a stirrer that follows a circular path. The bottom and top halves of the vessel is filled with heavy Bingham and light Newtonian fluids. We investigated the effect of the viscosity ratio on the fluid flow and mixing evolution.

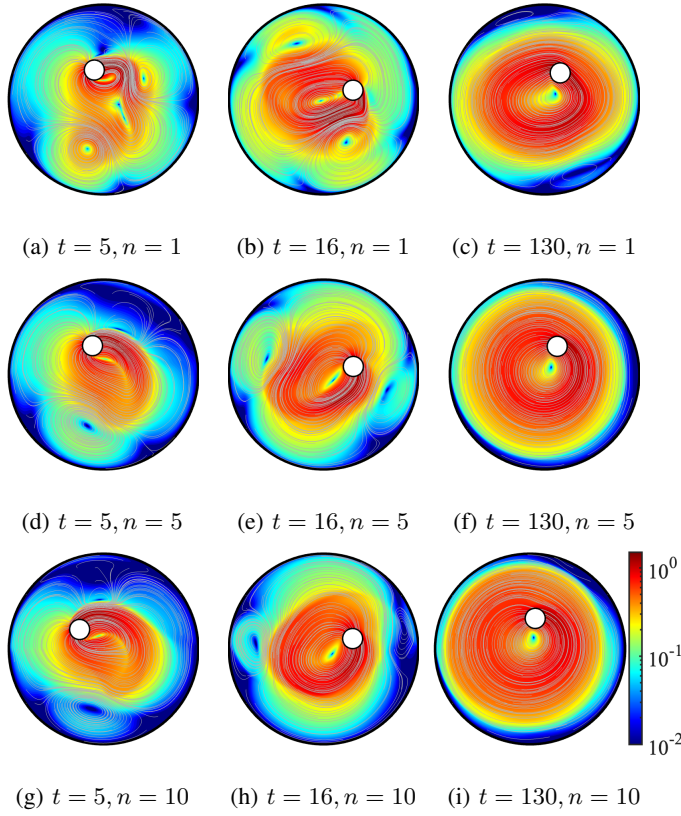


Fig. 8: Snapshots of the velocity magnitude for different viscosity ratios. The gray lines represent the streamlines.  
 $(Re = 2.7 \times 10^2, Bn = 5 \times 10^{-1}, Pe = 10^{10}, Ri = 10^{-2}, At = 10^{-2})$

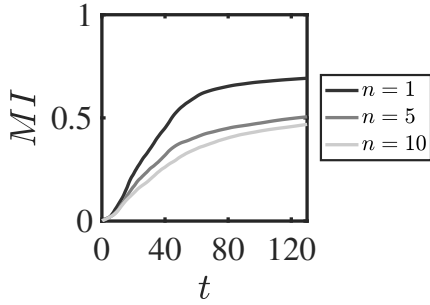


Fig. 9: Evolution of overall mixing index in different viscosity ratios.  
 $(Re = 2.7 \times 10^2, Bn = 5 \times 10^{-1}, Pe = 10^{10}, Ri = 10^{-2}, At = 10^{-2})$

We found that the formation of vortices plays an important role in mixing. As the viscosity ratio increases, the vortices near the vessel's wall become weaker, and the chaotic mixing zone gradually shrinks.

Moreover, it is found that as the viscosity ratio increases, more time is needed to reach the desired amount of mixing.

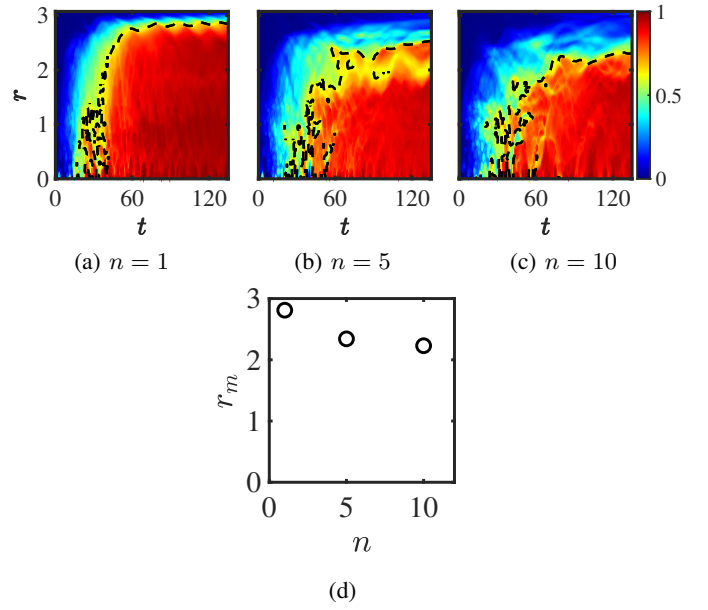


Fig. 10: (a-c) Spatio-temporal diagrams of  $\theta$ -averaged mixing index for different viscosity ratios. (d) Averaged radius of the mixed region.  
 $(Re = 2.7 \times 10^2, Bn = 5 \times 10^{-1}, Pe = 10^{10}, Ri = 10^{-2}, At = 10^{-2})$

## REFERENCES

- [1] Gouillart, E., Thiffeault, J.L. and Dauchot, O., 2010. Rotation shields chaotic mixing regions from no-slip walls. *Physical review letters*, 104(20), p.204502.
- [2] El Omari, K., Younes, E., Burghilea, T., Castelain, C., Moguen, Y. and Le Guer, Y., 2021. Active chaotic mixing in a channel with rotating arc-walls. *Physical Review Fluids*, 6(2), p.024502.
- [3] Aref, H., Blake, J.R., Budišić, M., Cardoso, S.S., Cartwright, J.H., Clercx, H.J., El Omari, K., Feudel, U., Golestanian, R., Gouillart, E. and Van Heijst, G.F., 2017. Frontiers of chaotic advection. *Reviews of Modern Physics*, 89(2), p.025007.
- [4] Gouillart, E., Kuncio, N., Dauchot, O., Dubrulle, B., Roux, S. and Thiffeault, J.L., 2007. Walls inhibit chaotic mixing. *Physical review letters*, 99(11), p.114501.
- [5] Boujlel, J., Pigeonneau, F., Gouillart, E. and Jop, P., 2016. Rate of chaotic mixing in localized flows. *Physical Review Fluids*, 1(3), p.031301.
- [6] Derksen, J.J., 2012. Direct simulations of mixing of liquids with density and viscosity differences. *Industrial & engineering chemistry research*, 51(19), pp.6948-6957.
- [7] Zare, M., Roustaei, A. and Frigaard, I.A., 2017. Buoyancy effects on micro-annulus formation: Density stable displacement of Newtonian-Bingham fluids. *Journal of Non-Newtonian Fluid Mechanics*, 247, pp.22-40.